Application of Aerosol Techniques to Study the Catalytic Formation of Methane on Gasborne Nickel Nanoparticles

Alfred P. Weber,* Martin Seipenbusch, and Gerhard Kasper

Institut für Mechanische Verfahrenstechnik und Mechanik, Universität Karlsruhe (TH), D-76128 Karlsruhe, Germany

Received: April 25, 2001; In Final Form: July 13, 2001

"Aerosol catalysis" is shown to be a powerful tool for investigating the catalytic properties of freshly formed nanoparticles in situ and without substrate interference. The method is first outlined conceptually, followed by an illustrative application to the catalytic formation of methane on a nickel nanoaerosol. Reaction order and activation energy were found conform with generally accepted values from supported Ni catalysts. The TOR decreases strongly during the first 10 s as the reaction proceeeds toward a steady value. The decrease correlates with a buildup of about 0.3 monolayer equivalents of carbon on the particle surface measured by TGA and a decline in particle photoelectric activity observed via measurement by aerosol photoemission spectroscopy (APES). APES is shown to be capable of detecting the progressive degradation of the freshly formed particle surface due to a heterogeneous surface reaction on a millisecond time scale. Furthermore, it was possible to induce order-of-magnitude changes in TOR via defined changes in particle morphology, induced by aerosol restructuring techniques preceding exposure to the catalytic reaction.

1. Introduction

In contemporary parlance, the "active phase" of a catalyst consists of nanoparticles. To preserve their high degree of dispersion and also to provide a suitable form of packaging and exposure in a chemical reactor, these nanoparticles are usually supported on much larger granules of an "inert" material such as Al_2O_3 or MgO. Experiments under real reaction conditions are usually done with such materials. However, supported catalysts are not ideal for investigating the fundamental properties of nanoparticles or materials because the various multistep methods for their preparation usually result in a loss of control over the size distribution and morphology of the nanophase and it also becomes difficult to separate the influence of the support material and other extraneous factors. Research has thus resorted to a variety of sophisticated tools for probing and modifying pure catalyst surfaces, many of which require ultrahigh vacuum to understand how molecules interact with catalysts.

Rapid advances during the past decade for preparing and handling "clusters" or "nanoparticles" have also opened up new avenues to study catalysts. Today, there we have an almost unlimited array of possibilities for making very well-defined particles from a few nanometers in diameter upward, especially by liquid-phase processes. This has also spurred fundamental investigations of unsupported colloidal catalysts. Schmid et al.,[1] for example, demonstrated how variations in size of ligand-stabilized metal clusters correspond to systematic changes in catalytic properties.

The aerosol route—often called gas-phase synthesis or chemical vapor synthesis in order to stress analogies with surface coating by CVD—provides another conceptually interesting approach to study unsupported as well as supported catalysts. For one, various types of techniques are available for on-demand production of well-defined nanoparticles in flow reactors, with high purity, and over a wide range of pressures. Aerosol conferences, workshops, and the pertinent archival literature give ample testimony to that effect. Second, one can proceed without removing these freshly generated particles from the gas stream to initiate a specific chemical reaction by mixing them in a second flow reactor with the required educt molecules and then continue to study its progress downstream. Since the reactor axis is in effect the reaction coordinate, one has a high degree of control over the size, morphology, and surface properties of the particulate phase. This represents some compensation for the fact that aerosols cannot be stabilized or manipulated as elegantly as colloids by means of electrical bilayers. More importantly, however, aerosol science has at its disposal a range of on-line tools for characterizing the particles, which offer unique ways to correlate particle properties with chemical kinetics and under actual process conditions, i.e., also at atmospheric or higher pressures. "Aerosol catalysis" may therefore eventually contribute to closing the so-called pressure gap between UHV methods of investigation and the real process and become another tool for catalyst development.

Despite its potential, the aerosol route with all its possibilities has so far not been used broadly, and pertinent literature is scarce. Glikin[2,3] has made extraordinary claims with regard to the effects of the aerosol state on the catalytic activity for the total oxidation of acetic acid over an iron oxide catalyst. However, it is doubtful whether the aerosols they used were sufficiently characterized and quantitatively understood. Nevertheless, these claims have contributed to sparking our own interest.[4]

The aim of this article is to demonstrate the possibilities of the aerosol technique by investigating a well know reaction, namely, the so-called methanation reaction over a Ni catalyst, i.e., the formation of methane from carbon monoxide and hydrogen.

* Corresponding author. E-mail: alfred.weber@ciw.uni-karlsruhe.de. FAX: 0049 721 608 6563.

10.1021/jp0115594 CCC: $20.00
Published on Web 09/06/2001

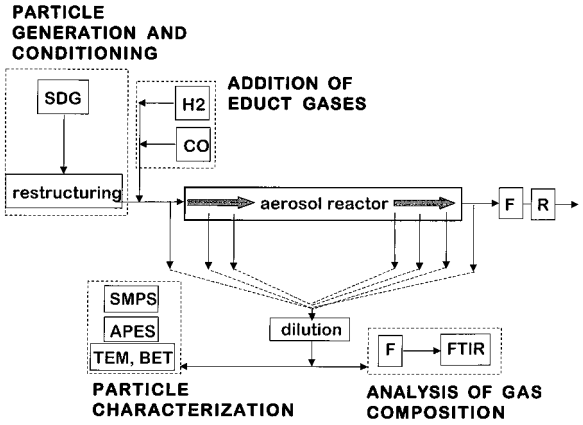

Figure 1. Schematic diagram of the experimental setup

2. Model Reaction $CO + 3H_2 \rightarrow CH_4 + H_2O$

The formation of methane from carbon monoxide and hydrogen over a Ni catalyst, the so-called methanation reaction was chosen as a simple and very well characterized system for which the literature offers ample data on classical supported catalysts. In addition, the rate of CH_4 formation can be translated directly into an overall turnover rate (TOR), defined as

$$\mathrm{TOR} = \frac{\text{number of product molecules}}{\text{number of active sites}\cdot\text{time}} \quad (1)$$

because methane is formed almost exclusively (>98%). The TOR is related to the reaction rate r, i.e., the volume of methane produced per mass of catalyst and time, in mL mg^{-1} s^{-1}

$$\mathrm{TOR} = \frac{rN_A}{V_M S_{BET} \delta} \quad (2)$$

where N_A is the Avogadro number, V_M the molar volume, S_{BET} the specific surface area of the catalyst, and δ the number of active sites per unit surface area.

The reaction order for hydrogen is known to be close to unity, while the reaction order for carbon monoxide is reported to vary between -1 and 0.5, depending on CO partial pressure.[5] However, by keeping the amount of produced methane low with low educt concentrations and short reaction times, the initial concentrations of CO and H_2 remain virtually constant throughout the reactor. Under these conditions, the reaction orders of the individual educt gases need not be considered for the determination of the TOR. They were determined nevertheless in separate experiments by varying the educt initial concentrations to establish a comparison with the classical route. Moreover, the overall activation energy for the formation of methane was determined from an Arrhenius-type plot.

3. Experimental Setup

As outlined above, the basic idea is to start with gasborne nanoparticles produced freshly in a continuous process, thereby guaranteeing constant and reproducible initial conditions. Immediately after generation, the aerosol may undergo modification steps to adjust particle structure and certain surface conditions (for which an operational definition shall be given later on) to have a broader range of variability than afforded by the generator alone. These particle properties are all measured and monitored as far as possible with on-line techniques, as described in Section 4. In a third reactor, the actual catalytic reaction is initiated and studied. A schematic diagram of the experimental setup is shown in Figure 1.

3.1. Aerosol Particle Generation. Nickel nanoparticles are generated with a spark discharge generator (SDG).[6] In this device, two Ni electrodes are placed in an inert gas stream (99.99% N_2). A capacitance of 20 nF parallel to the electrodes is periodically charged by a constant current until the breakthrough voltage is reached. The ensuing spark vaporizes small but fairly constant amounts of metal, which then form Ni nanoparticles of about 4 nm diameter by homogeneous nucleation. These so-called primary particles undergo collisions resulting in chainlike agglomerates in the size range of tens to a few hundred nanometers (Figure 2a). The agglomerate number concentration is controlled by the discharge frequency and was in the range of 5×10^6 cm^{-3}. On-line measurements with a scanning mobility particle sizer (SMPS) give continuous data on agglomerate size distribution and number concentration.

3.2. Structure Modification of the Agglomerates. As illustrated in Figure 2a, the Ni agglomerates have a high porosity, i.e., a large percentage of exposed surface area. One can rearrange the primary particles to form more compact agglomerates with only minor loss of overall BET-equivalent surface area (Figure 3). This "restructuring" is induced thermally by passing the aerosol through a heated tube furnace. Once mobile enough to move, the primary particles rearrange into a lower energy state, i.e., in a more compact agglomerate structure,[7] as illustrated in Figure 2b. Above about 450 °C, one observes the onset of sintering accompanied by a rapid decrease of BET surface area, followed by melting of the nickel, which ultimately leaves solid spherical particles (see Figure 2c,d). At the exit of the furnace, the aerosol is at room temperature.

The exposed surface area per average particle shown in Figure 3 is determined from its mobility equivalent size measured by electrical mobility analysis (see below), which is known to be a good representation of projected area.[8,9]

3.3. Catalysis. After conditioning, the educt gases CO and H_2 are added to the aerosol immediately before entering the flow reactor, which is heated, thereby initiating the catalytic reaction. The point at which a constant maximum temperature is reached is defined as $t = 0$ for the reaction. Changing gas composition and particle properties are monitored by a succession of sampling points which correspond to residence times between a few seconds and a few minutes. At that point, the reaction and any further growth processes within the aerosol are quenched by dilution with a known flow of nitrogen, and the aerosol sample is split for particle characterization and for gas analysis. The aerosol characterization will be discussed below. For the gas analysis, the particles are first removed by filtration, and the gas composition is then determined on-line with an FTIR spectrometer (Bruker Model Vector 22) equipped with an 8.8 m cell. Stable concentrations in the optical cell were obtained about 5 min after a change in input conditions, corresponding to three exchanges of the cell volume.

4. Particle Characterization Techniques

The Ni particles were characterized by on-line and off-line techniques. The latter include total surface area determination by standard nitrogen adsorption (BET, Quantachrom Nova 2000), transmission electron microscopy (TEM, Zeiss Leo EM 109), and thermogravimetric analysis (TGA, Netsch TG 209) coupled with an FTIR spectrometer to analyze adsorbates on the particle surface qualitatively and quantitatively.

Aerosol particle size distributions and concentrations were principally determined on-line by a scanning mobility particle sizer (SMPS, combining TSI Models 3071 and 3022). This technique is based on fractionating particles according to their

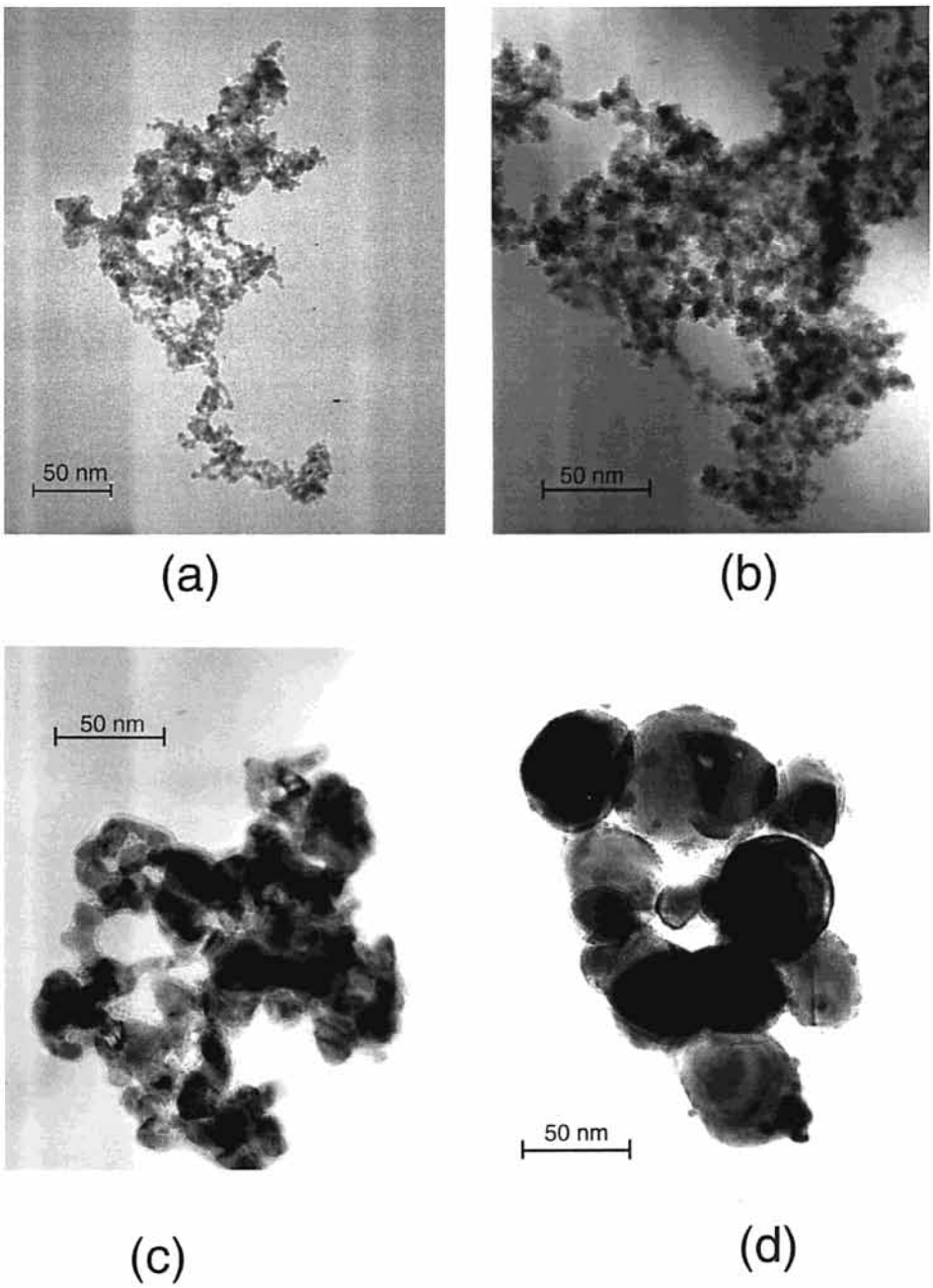

Figure 2. (a) Agglomerate of Ni nanoparticles at room temperature. (b) Collapsing of the agglomerate after heating to 450 °C. (c) Partial sintering of the agglomerate after heating to 600 °C. (d) High degree of sintering after heating to 900 °C, but complete sintering of the agglomerate to a spherical particle is not achieved yet

mobility in an electric field and is amply described in the literature.[10,11]

4.1. Aerosol Photoemission Spectroscopy (APES). Since its first introduction,[12] APES has become a valuable tool for probing the surface of particles in their gas-borne state. APES is based on photon-induced electron emission from the particle surface, which leads to a stable charge level on the aerosol that is determined on-line via simultaneous measurements of total electrical charge and total particle number concentration. For small particles (<300 nm), the escape probability of the photoelectron is close to unity,[13] even at atmospheric pressure. Aside from its dependence on particle surface area (and hence size), the electron emission yield, expressed as average number of unit charges per particle, is a highly sensitive function of both surface composition and photon energy. APES is therefore an ideal tool to track changes in particle surface, either during the generation and conditioning process or, subsequently, during participation in the catalytic reaction.

The photoelectric yield Y is the probability, per incident photon of energy $h\nu$ above the photothreshold Φ, of emitting an electron from a particle. In the vicinity of the photothreshold, Y is given by the Fowler−Nordheim equation function[14]

$$Y = c(h\nu - \Phi)^m \tag{3}$$

where $m = 2$ holds for metallic particles or graphite. In practice, c and Φ are determined by plotting $\sqrt{Y}$ over a range of energies $h\nu$. The emission constant c is proportional to the local density of states at the Fermi level; Φ is an effective work function. Changes in surface chemical composition by reaction or adsorption may affect the work function Φ and/or the local density of states and hence c. Because of the nonideal nature

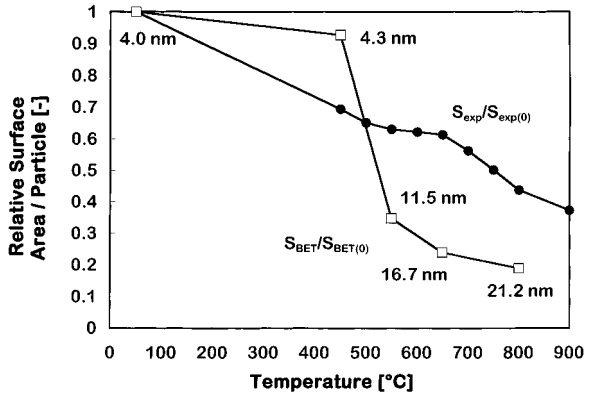

Figure 3. Exposed surface area (based on mobility equivalent diameter) and total surface area (based on BET) of agglomerates of Ni nanoparticles as a function of temperature. The numbers along the curve give the primary particle size.

of an aerosol system, there is no established theoretical correlation, but a great deal of empirical work has been done, especially related to combustion[15] and adsorption,[16] which has proven APES to be a very sensitive technique to track and in some cases quantify changes occurring on the surface. However, APES has, to our knowledge, not been correlated with catalytic activity.

In practice, Φ and c are determined from the electron emission rate per particle for a given irradiation spectrum (also called photoelectric activity):

$$\frac{I\Delta t}{N} = YF_{\mathrm{D}}S_{\mathrm{p}} \tag{4}$$

where F_{D} is the photon flux density and S_{p} the particle surface relevant for photoemission. Initially, uncharged gas-borne nanoparticles are irradiated for a fixed period of time Δt (well below any saturation effects) with monochromatic photons from a broad-band UV source coupled with a monochromator. The photon flux incident on the particles is measured with a UV-sensitive photomultiplier. The irradiation time Δt is given by the residence time in the photo chamber. The resulting net average charge per particle, a direct measure for the yield, is determined from simultaneous measurements of the aerosol current I with a Faraday cup electrometer (FCE) and the total number concentration N with a condensation particle counter (CPC).[17]

Equation 4 further requires a value for the surface area per particle, S_{p}. It has been shown [18] that the mobility equivalent diameter of an agglomerate particle as determined by SMPS is the appropriate measure for the exposed surface area and hence also for the surface available to photoemission. This was confirmed in earlier experiments[19] with agglomerates of Pt primary particles. When applying the thermal restructuring technique described above to these agglomerates, it was indeed found that the photon induced average charge per particle remained proportional to the square of the mobility equivalent diameter, as long as c and Φ were constant.

4.2. Relationship between APES and Catalytic Activity. In the following discussion of the particle properties, extensive use will be made of the correlation between photoelectric and catalytic activity. The reason these two activities are, at any time, proportional to each other is that both are directly related to the local density of states (LDOS) at the Fermi energy level. On one hand, the possibility for the emission of a photoelectron (given by the emission constant) is determined by the LDOS (E_{F}). On the other hand, main steps in the course of a catalytic reaction depend directly on the LDOS (E_{F}).[20] This correlation is shown in Figure 4, which will be discussed below.

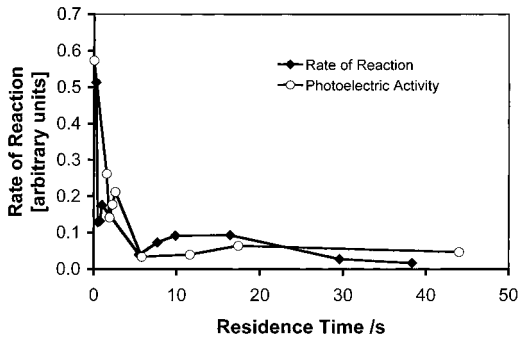

Figure 4. Temporal evolution of the photoelectric and catalytic activity of unconditioned Ni nanoparticles (reaction temperature of 450 °C).

5. Results and Discussion

5.1. Reaction Order and Activation Energy. The order of a reaction α_i with regard to constituent i is obtained by plotting the reaction rate r versus partial pressure of this constituent. For α_{CO}, the results obtained in our reactor are shown below in Table 1 for Ni aerosol coming directly from the spark discharge generator without any restructuring. The values range from -0.52 to -0.15 and evidently fall within the range published for supported Ni catalysts.

Similarly, the activation energy agreed well with literature values for temperatures of up to 350 °C, as shown in Table 2 below.[4]

TABLE 1: Reaction Orders for CO on Ni Aerosol Catalysts

partial pressure of CO [Pa]	reaction order of CO [−]
5250	−0.15
7210	−0.48
11 010	−0.52

TABLE 2: Activation Energies Measured with Ni Aerosol Compared to Literature for Supported Catalysts

	catalyst type	activation energy [kJ/mol]
this work[4] ($T \leq 350$ °C)	aerosol	96
Vannice[21]	supported	103
Vannice[21]	supported	107
Goodman[22]	supported	109

Above 350 °C, the activation energy and the reaction rate becomes progressively smaller than those extrapolated from the lower temperature behavior due to the accelerated formation rate of adsorbed carbon atoms on the catalyst surface. If the hydrogenation rate cannot keep up with the dissociation of CO at higher temperatures, carbon builds up on the particle surface, which may transform into graphite. Goodman[22] found that the formation of relatively inactive graphite on a single-crystal nickel catalyst requires both a critical temperature of 375 °C and a prerequisite surface carbide level. As will be shown below, a buildup of carbon on the surface of our Ni aerosol particles was indeed observed. In summary, these findings indicate that the key features of the methanation reaction (i.e., overall activation energy, reaction order and poisoning effects) are similar for supported and gas-borne catalyst particles.

5.2. Temporal Evolution of Catalytic and Photoelectric Activity. As mentioned above, the catalytic activity of Ni aerosol particles drops substantially above 350 °C due to the "poisoning" by adsorbed carbon. The kinetics of such a poisoning is shown in Figure 4. Beside the temporal evolution of the catalytic activity of Ni nanoparticles during the methanation reaction at

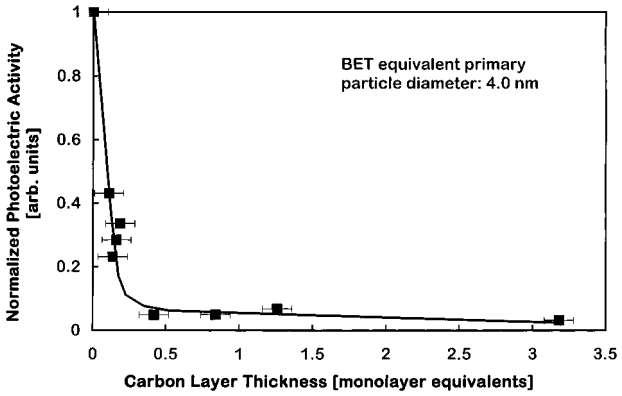

Figure 5. Photoactivity vs the amount of carbon deposited on the particles (reaction temperature of 450 °C).

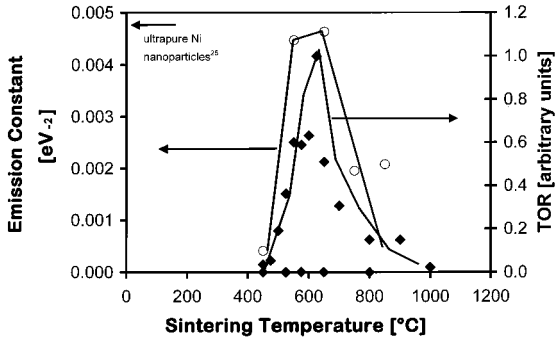

Figure 6. Catalytic and photoelectric activity as a function of particle preconditioning temperature (residence time of 38 s).

450 °C, the photoelectric activity is shown also. The catalytic activity decreases substantially over a few seconds. After about 5 s, the reaction rate approaches a constant value, however, at a low level compared to the initial activity. The initial decay of the catalytic activity during the first seconds is enormous. However, the amount of methane produced in the first milliseconds is so small that a direct detection with FTIR is beyond the measuring capabilities. With the current setup, the shortest measured residence time was 250 ms. Here, as an alternative, the correlation between photoelectric and catalytic activity[17] can be used. This means that instead of measuring the amount of catalytically produced gas-phase products, the activity of the particles is determined over the photoelectric activity. This approach should thus be capable, providing a measure for the activity of freshly formed surfaces on a time scale of as low as a few milliseconds.

To investigate the influence of the deposited carbon on the photoelectric behavior, samples were taken after different residence times in the reactor and analyzed by APES and for carbon content. The amount of carbon deposited on the nanoparticle agglomerates was measured by TGA and FTIR. The results are shown in Figure 5. The amount of carbon is translated into a monolayer equivalent, i.e., the number of monolayers if the carbon atoms would be distributed homogeneously over the total particle surface. It is obvious from Figure 5 that a drastic decrease of the photoactivity occurs when carbon deposition starts. At several monolayers, the photoelectric behavior of the Ni particles approaches the one of graphite particles. The interesting point is that less than one monolayer equivalent is needed to reduce the photoactivity and, therefore, the catalytic activity of the nanoparticles successfully. This indicates that even at this small scale the surface of 4 nm particles contains sites of higher and lower activity. The carbon seems to deposit on the active sites first leading to a very efficient poisoning of the catalyst.

5.3. Influence of Agglomerate Structure Modification on Catalytic Activity. So far, the behavior of untempered particles has been studied. Next, the influence of the reduction of the BET surface, i.e., the increase of primary particle size, at constant aerosol mass concentration on the catalytic activity will be discussed. Since the temperature in the reactor was 450 °C, restructuring effects below this temperature were not investigated. As shown in Figure 3 for temperatures above 450 °C, only moderate changes of the agglomerate mobility were observed, indicating that the apparent projection area of the agglomerate was only reduced by a little. However, for temperatures above 450 °C, a significant decrease of the specific surface area was found, which is related to an increase of the primary particle size. Figure 6 shows the catalytic and photoelectric activity as a function of temperature, to which the particles were exposed before reaction. As known from former work by Schmidt-Ott et al.,[23] the photoelectric activity, which is correlated to the catalytic one, is reduced for decreasing mobility equivalent diameter. However, in our case, the catalytic activity even increases when the mobility diameter decreases in the temperature range from 450 to 600 °C. Therefore, this increase cannot be related to structural changes of the agglomerates. The explanation may rather be related to the impurities in the nickel (<1%). It is known that at elevated temperatures impurities can move to the particle surface. This cleaning of the particle interior is even more pronounced for nanoparticles.[24] We hypothesize that the impurities may desorb or react and desorb from the Ni surface resulting in cleaner catalytic particles. This hypothesis is supported by the APES measurements, which show for the particles heated to 600 °C emission constants close to the value reported for ultrapure Ni nanoparticles.[25]

For temperatures above 625 °C, the catalytic activity decreases substantially with temperature, although no significant change of mobility diameter or of the specific surface area has been observed. Therefore, this decrease can be related to internal changes only. In fact, Baumann[26] reports that metal particles approaching their sintering temperature can undergo changes of the crystalline structure resulting in a decreased photoactivity. For nanometer particles, the sintering temperature may be reduced by several hundred degrees compared to the bulk melting point. Since photoactivity and catalytic activity are correlated via the local density of states at the Fermi energy level, such changes of the crystal structure would affect the catalytic activity of nanoparticles in the same way.

In any case, it is obvious that the particle history can have an important influence on their catalytic performance.

Summary and Conclusions

A new approach to on-line investigations of heterogeneous catalytic reactions on gasborne nanoparticles is presented. It combines particle formation, restructuring and measurement techniques via the aerosol route to obtain well-defined nanoparticle properties with measurements of gas phase composition by FTIR spectroscopy. Time-resolved measurements in a flow reactor permitted observation of the kinetics of catalyst deactivation due to the formation of submonolayers of carbon. It was possible to correlate the resulting decline in TOR with a change in particle photoelectric activity, measured in real time by APES. In addition, the influence of deliberately imposed changes in particle morphology on the catalytic performance was observed.

"Aerosol catalysis" is first of all shown to be a new tool for understanding the relationship between particle properties and

catalytic activity. It has potential for developing new catalysts and may also be an avenue for investigating the putative relationship between combustion aerosols and the formation of dioxin.[27]

Acknowledgment. The financial support of this project by the Ministerium für Wissenschaft und Kunst des Landes Baden-Württemberg, Germany, within the interfacultative research group "Nanotechnology-controlled functional elements on the nanometer scale" is highly appreciated.

References and Notes

(1) Schmid, G.; Maihack, V.; Lantermann, F.; Peschel, S. *J. Chem. Soc., Dalton Trans.* **1996**, *5*, 589.
(2) Glikin, M. A. *Theor. Found. Chem. Eng.* **1996**, *30*, 390.
(3) Glikin, M. A.; Kutakova, D.; Prin, E. *Chem. Eng. Sci*. **1999**, *54*, 4337.
(4) Weber, A. P.; Seipenbusch, M.; Thanner, Ch.; Kasper, G. *J. Nanoparticle Res.* **1999**, 1, 253.
(5) Klose, J.; Baerns, M. *J. Catal*. **1984**, *85*, 105.
(6) Schwyn, S.; Garwin, E.; Schmidt-Ott, A. *J. Aerosol Sci*. **1987**, *19*, 639.
(7) Weber, A. P.; Friedlander, S. K. *J. Aerosol Sci.* **1997**, *28*, 179.
(8) Rogak, S. N.; Flagan, R. C.; Nguyen, H. V. *Aerosol Sci. Technol*. **1993**, *18*, 25.
(9) Katzer, M.; Weber, A. P.; Kasper, G. *J. Aerosol Sci*., in press.
(10) Wang, S. C.; Flagan, R. C. *Aerosol Sci. Technol*. **1990**, *13*, 230.
(11) Fissan, H.; Hummes, D.; Stratmann, F.; Büscher, P.; Neumann, S.; Pui, D. Y. H. Chen, D. *Aerosol Sci. Technol.* **1996**, *24*, 1.
(12) Schmidt-Ott, A.; Schurtenberger, P.; Siegmann, H.-C. *Phys. Rev. Lett*. **1980**, *45*, 1284.
(13) Filipov, A.; Schmidt-Ott, A.; Fendel, W. *J. Aerosol Sci*. **1993**, *24*, S501.
(14) Schleicher, B.; Burtscher, H.; Siegmann, H.-C. *Appl. Phys. Lett*. **1993**, *63*, 1191.
(15) Burtscher, H. *J. Aerosol Sci*. **1992**, *23*, 549.
(16) Burtscher, H.; Schmidt-Ott, A. *J. Aerosol Sci*. **1986**, *17*, 699.
(17) Weber, A. P.; Seipenbusch, M.; Kasper, G. *Chem. Ing. Technol*. **2000**, 72 (8), 879.
(18) Schmidt-Ott, A.; Baltensperger, U.; Jost, D. T.; Gäggeler, H. W. *J. Aerosol Sci*. **1990**, 21, 711.
(19) Weber, A. P.; Burkert, K.; Kasper, G. *AIChE Proc*. **1998**, *1*, 285.
(20) Thomas, J. M.; Thomas, W. J. *Principles and Practice of Heterogeneous Catalysis*; VCH: Weinheim, Germany, 1997.
(21) Vannice, M. A. *Catal. Rev. Sci. Eng*. **1976**, *14*, 153.
(22) Goodman, D. W.; Kelley, R. D.; Madey, T. E.; Yates, J. T., Jr. *J. Catal*. **1980**, *63*, 226.
(23) Schmidt-Ott, A. *J. Aerosol Sci*. **1988**, *19*, 553.
(24) Weller, H. *Curr. Opin. Colloid Interface Sci*. **1998**, *3*, 194.
(25) Müller, U.; Ammann, M.; Burtscher, H.; Schmidt-Ott, A. *Phys. Rev. B* **1991**, 44(15) , 8284.
(26) Baumann, F. *Z. Physik* **1960**, *158*, 607.
(27) Huang, H.; Buekens, A. *Chemosphere* **1995**, *31*, 4099.